(A run group proposal to Jefferson Lab PAC49)

TDIS-n: Tagged DIS measurement of the Neutron Structure Function

Carlos Ayerbe Gayoso (spokesperson)
Helmholtz Institute Mainz. Johannes Gutenberg University, 55099 Mainz, Germany
and Mississippi State University, Mississippi State, MS 39762

Eric Fuchey (spokesperson)
University of Connecticut, Storrs, CT 06269

Rachel Montgomery (spokesperson)
SUPA School of Physics and Astronomy, University of Glasgow, Glasgow G12 8QQ, UK

Cynthia E. Keppel (spokesperson), Arun S. Tadepalli (spokesperson), David Gaskell, Stephen Wood
Thomas Jefferson National Accelerator Facility, Newport News, VA 23606

John Arrington (spokesperson), Shujie Li (spokesperson)
Lawrence Berkeley National Laboratory, Berkeley, CA 94720

Paul E. Reimer
Argonne National Laboratory, Argonne, IL 60439

Deepak Bethuwal, Hem Bhatt, Bhesha Devkota, Jim Dunne, Dipangkar Dutta, Lamiaa El-Fassi, Abishek Karki
Mississippi State University, Mississippi State, MS 39762

Wenliang B. Li
William & Mary, Williamsburg, VA 23185

and

The TDIS Collaboration

April 2021

Contents

1 Executive Summary

We propose to extract the free neutron structure function from electron-deuterium scattering using a time projection chamber to detect low-momentum spectator protons, identifying nearly on-shell nucleons. This experiment will use the same SBS experimental setup and beam time as the Conditionally Approved Hall A TDIS experiment (E12-14-010). Spectator proton tagging using the mTPC isolates scattering from the neutron, removing the need for subtraction of large proton contributions, and allowing us to determine and correct for the initial struck neutron momentum. This reduces Fermi smearing corrections, both at large x and in the resonance region, where these corrections are most important. Using this technique, inclusive measurements can be made covering the DIS region, the resonance region, and elastic e-n scattering.

TDIS-n will reach Q^2 values of 6-7 GeV^2 with a statistical accuracy of better than 3% at the large x. This allows us to make several interesting physics measurements:

- A high-statistics extraction of $F_2^n(x)/F_2^p(x)$ for $0.3 < x < 0.7$ with completely different systematic uncertainties than the recent result from MARATHON [1] and different systematics plus new tagging efficiency studies compared to BoNuS12 [2].
- High-statistics measurements of F_2^n (and F_2^p) in the resonance region Q^2 from 2-7 GeV^2. This provides a comparison of resonance production off the neutron and the proton, and will allow us to determine if the falloff of the Δ resonance in e-p scattering is also observed in scattering from the neutron.
- The tagged neutron measurements will allow us to measure the elastic electron-neutron cross section and extract the magnetic form factor without the need for subtracting proton contributions (as for e-d quasielastic measurements) and without having to correct for a neutron detection efficiency.
- Combining the tagged neutron structure function measurement with inclusive data from the proton and deuteron, TDIS-n will extract of the "EMC effect" for the deuteron, i.e. $F_2^d/(F_2^p + F_2^n)$, in a way that allows for cancellation of several systematics in the measurements.

In most cases, similar measurements exist or are planned, but TDIS-n can still make important contributions in each of these areas. In particular, BoNuS12 will use a similar technique and also has a larger electron acceptance coverage for tagged e-n scattering. While our Q^2 range is limited to smaller scattering angles, our yield will be a factor of 7 higher compared to the BoNuS12 proposal, allowing for higher statistics (and additional systematic studies) in our kinematic region. This will allow for DIS and resonance region F_2^n measurements with higher stastics than any existing or planned tagged measurements, and without the need for nuclear corrections and proton subtraction that limit measurements from F_2^d. For the e-n elastic scattering, the tagged measurements will have entirely different systematic uncertainties from the one precision data set at large Q^2 values [3] and future measurements in Halls A and B, all of which extract G_{Mn} from the ratio $d(e,e'n)/d(e,e'p)$. In the DIS region, our extraction of F_2^n/F_2^p will have completely different systematics compared to the MARATHON experiment and with independent checks on the efficiency of the tagging as well as new studies of the off-shell effects in the region of interest, as described below.

In addition, we can provide never-before performed measurements of the spectator tagging technique. First, we can make an absolute calibration of the tagging efficiency based on an independent measurement - elastic e-n scattering with neutrons detected in the hadron calorimeter (HCAL) - while BoNuS had to rely on normalizing the data to reproduce previous extractions of F_2^n/F_2^p at kinematics where the model dependence was small. We will also have the statistics to examine the DIS structure function at modest x values as a function of the spectator proton momentum, rather than integrating over the full 60-100 MeV/c range where off-shell effects and final state interactions are predicted to be small, as discussed in Sec. 3.3. This will provide a direct test of the models of off-shell effects and final state interactions used to determine the model dependence in the extraction of the free neutron structure from tagged neutrons.

2 Introduction

The proton and neutron (also called nucleons) are the basic building blocks of matter. It is well known that they are not elementary particles, but a complex and dynamic composite of quarks and gluons, and as such also represent some of the most basic (and accessible) bound states of QCD. While a wealth of information is available on the proton, precise and model independent information on the neutron is essential for a thorough understanding of nucleon structure.

Due to the lack of a free neutron target, (short lifetime of $\sim$<15 minutes) our understanding of neutron structure has to be deduced from measurements on light nuclei such as ^{2}H and ^{3}He, where corrections have to be made for the larger cross section contributions from the protons and for nuclear effects in these targets. Recently, experiments conducted in Hall B of Jefferson lab on the deuteron, such as BoNuS, seek to minimize the model dependencies by tagging low-momentum recoiling protons to ensure that the struck neutron was nearly on-shell.

An improved measurement of the neutron structure function can provide insight into the flavor structure of the nucleon, while clean measurements of resonance production from the nucleon can be used to constrain the isospin dependence in resonance production. Our proposed tagged measurements will provide clean information on the neutron structure function, with a luminosity that will allow for a significant improvement in the statistics in the x and Q^2 range accessible to our experiment, in particular at large x values for Q^2 up to 6-7 (GeV/c)^2. In addition, TDIS-n will provide an independent measurements of the tagging efficiency, not possible with BoNuS12, and will study the off-shell corrections by examining F_2^n as a function of spectator momentum using data in our highest statistics region.

3 TDIS-n Overview

In the following section, we summarize the physics motivation, experimental technique, and model-dependent corrections associated with the tagged measurements of the neutron structure. The details of the experimental setup and detector performance are covered in the following section.

3.1 Physics motivation

Spectator tagging provides an effective way to measure inclusive scattering from a nearly on-shell neutron, providing access to the neutron structure function and form factors. We provide below a brief overview of the physics accessible by applying this technique to scattering in the DIS region, the resonance region, and in elastic e-n scattering.

We note that the BoNuS12 experiment [2] will make similar tagged measurements of the free neutron structure function, but with a factor of 5-10 less statistics in the kinematics that overlap the TDIS-n measurement, as described in Sec. 7, and without the benefit of an independent measurement of the tagging efficiency as presented in Sec. 5.3.4. Therefore, even in the region of overlap, the TDIS-n measurement will provide additional statistics and independent tests of the systematics associated with tagged measurements on the deuteron, of relevance both at Jefferson Lab [2, 4] and the EIC [5, 6].

3.1.1 Deep Inelastic Scattering from the neutron

The pioneering inclusive electron scattering experiments at SLAC in 1960s showed that the proton is a composite system. The differential DIS cross section could be written as:

$$\frac{d^2\sigma}{d\Omega dE'} = \left(\frac{d\sigma}{d\Omega}\right)_{\text{Mott}} \left[W_2(Q^2,\nu) + 2W_1(Q^2,\nu)\tan^2\frac{\theta}{2}\right] . \quad (1)$$

with, $(\frac{d\sigma}{d\Omega})_{\text{Mott}}$ the point-like Mott cross-section, θ the electron scattering angle, $Q^2 = 4EE'\sin^2\frac{\theta}{2}$ the 4-momentum transfer squared, $\nu = E - E'$ the energy transfer, and $W_{1,2}$ are called response functions (W_1 electric interaction and W_2 magnetic interaction).

Under impulse approximation, in the infinite momentum frame, Bjorken [7] showed that these response functions could be written as dimensionless functions, called Structure Functions (SF), which depend on Q^2 and a new variable, $x = \frac{Q^2}{2M\nu}$:

$$F_1(Q^2, x) = MW_1(Q^2, \nu)\ ; \qquad F_2(Q^2, x) = \nu W_2(Q^2, \nu)\ . \tag{2}$$

Even more, Bjorken demonstrated that in the deep inelastic regime ($Q^2 \to \infty, \nu \to \infty,$), $F_{1,2}$ are independent of Q^2 and just scale as a function of x.

In the Parton-Quark model by Feynman, Bjorken and Paschos [8, 9], the information is contained in the Parton Distributions Functions (PDFs) which are related to the unpolarized structure as a linear combination of the PDFs: $F_1(x) = 1/2\sum_i e_i^2 f_i(x)$, with e_i the i-parton electric charge and $f_i(x)$ the i-PDF[1]. In this scenario $F_1(x)$ and $F_2(x)$ are related through the Callan-Gross relation[2] $F_2(x) = 2xF_1(x)$. Expanding $F_2(x)$ for the proton and neutron into their light quark content[3], and that the strange quark content is small and negligible, we obtain:

$$\frac{F_2^p(x)}{x} = \left(\frac{4}{9}u(x) + \frac{1}{9}d(x)\right)\ ; \qquad \frac{F_2^n(x)}{x} = \left(\frac{4}{9}d(x) + \frac{1}{9}u(x)\right)\ . \tag{3}$$

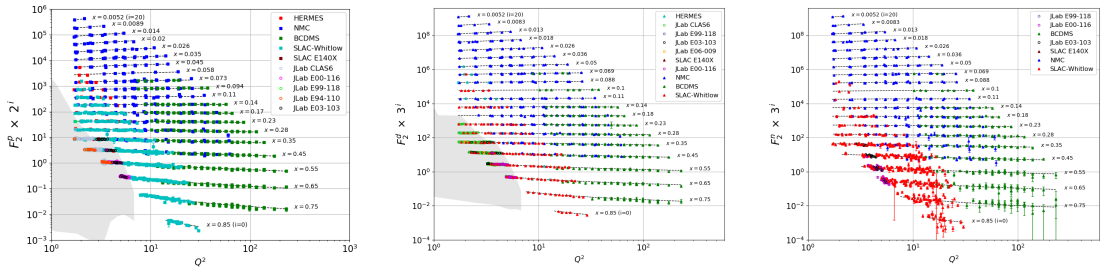

Figure 1: Measured values of F_2^p (left panel) and F_2^d (middle panel) together with the CJ15 fit, as a function of Q^2 at fixed x. The data have been scaled by a factor 3^i, from $i = 0$ for $x = 0.85$ to $i = 20$ for $x = 0.005$ [10]. The shade indicates available resonance data. The right panel shows F_2^n extracted from the proton and deuteron measurements [11].

A compilation of the extensive proton and deuteron SF data is shown in Fig. 1, along with the neutron SF data set extracted from the proton and deuteron data. The neutron SF has the same wide kinematic coverage as proton and deuteron, but because $F_2^n(x) \approx F_2^d(x) - F_2^p(x)$, the uncertainty in $F_2^n(x)$ is significantly enhanced by the subtraction of the dominant proton contribution. There are additional corrections associated with the binding and motion of the neutrons in the deuteron. For instance, although the deuterium is a weakly bound system, binding and Fermi momentum introduce significant model dependence in the extraction of $F_2^n(x)$ at large x, with additional model dependence at all x associated with the off-shell corrections applied or, alternatively, the extrapolation of the EMC effect to the deuteron (see Sec. 3.3 and Refs. [12, 13]). The impact of the large proton subtraction and model-dependent corrections is reflected in the much larger uncertainties for F_2^n, clearly visible in the large x region.

[1] it is implicit from now on that $f_i(x) \equiv f_i(x) + \overline{f_i}(x)$

[2] valid for partons with spin 1/2

[3] assuming isospin symmetry, $u(x) \equiv u_p(x) = d_n(x)$ and $d(x) \equiv d_p(x) = u_n(x)$

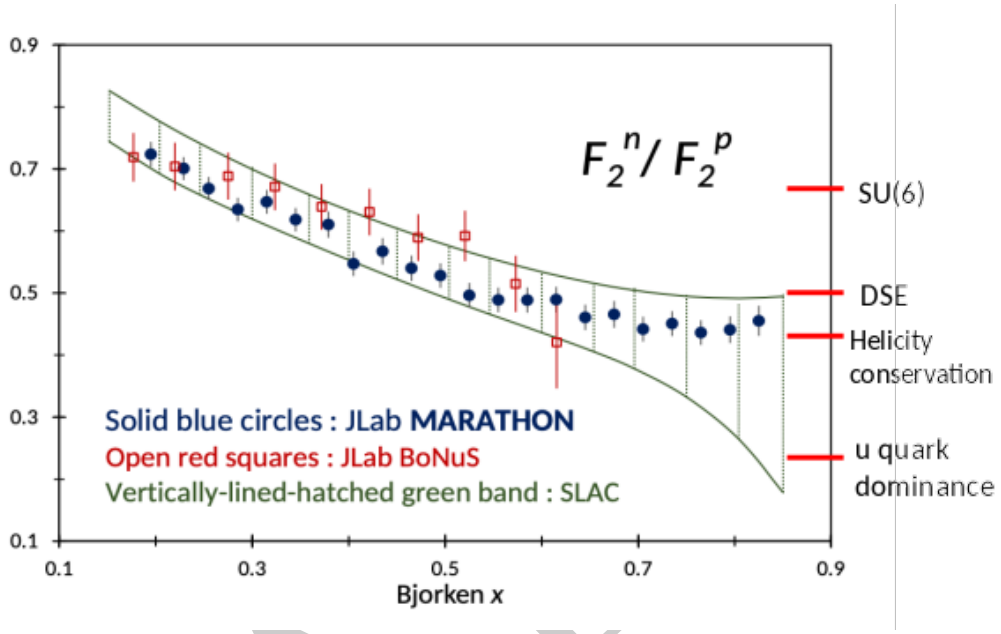

Figure 2: F_2^n/F_2^p ratio from MARATHON [1], BoNuS [14], and the uncertainty region from SLAC experiments [15]. The d/u predictions are shown for $x \to 1$: SU(6) spin-flavour symmetry, perturbative QCD [16] (which predicts $F_2^n/F_2^p \to 1$), Hyperfine Structure Effect [17], and predictions from the Dyson-Schwinger equation (DSE) for two computational cases [18].

Several nucleon structure models, instead of predicting the behaviour of the single PDF when $x \to 1$, focus on predictions for the $d(x)/u(x)$ ratio yielding the predictions for F_2^n/F_2^p shown in Fig. 2. To leading order, the d/u ratio can be extracted from knowledge of the proton and neutron SF as shown in eq. 4:

$$\frac{F_2^n(x)}{F_2^p(x)} \approx \frac{1+4d/u}{4+d/u} \Rightarrow \frac{d}{u} \approx \frac{4F_2^n/F_2^p - 1}{4 - F_2^n/F_2^p} \ . \tag{4}$$

While our measurement will not add new data the high-x region, we provide an independent check of the normalization procedure used in BoNuS and MARATHON, shown in Fig. 2, and planned for BoNuS12. While these are "model-independent" extractions, in that they do not rely on extracting the neutron from inclusive measurements on the proton and deuteron (or ^{3}He), they all require independent normalization of the data against measurements at $x \approx 0.3$, where the model dependence of the deuteron measurements is believed to be understood. The TDIS-n extraction can take the same approach, but we will also measurement of the tagging efficiency by identifying events with spectator protons using the over-constrained $d(e,e'n)p_s$ reaction, with the neutron measured in the SBS hadron calorimeter (HCAL).

3.1.2 'EMC effect' in the deuteron

As noted above, neutron information comes mainly from bound systems due to the non-existence of free neutron targets, mainly ^{2}H or ^{3}He, which introduces several sources of uncertainty such as Fermi motion, off-shell effects, final-state interactions or the EMC effect, which can influence the extraction [19, 20, 21, 22]. These model uncertainties, discussed in detail in Sec. 3.3 can be greatly reduced by use of spectator tagging, as demonstrated in the BoNuS experiment[23, 14].

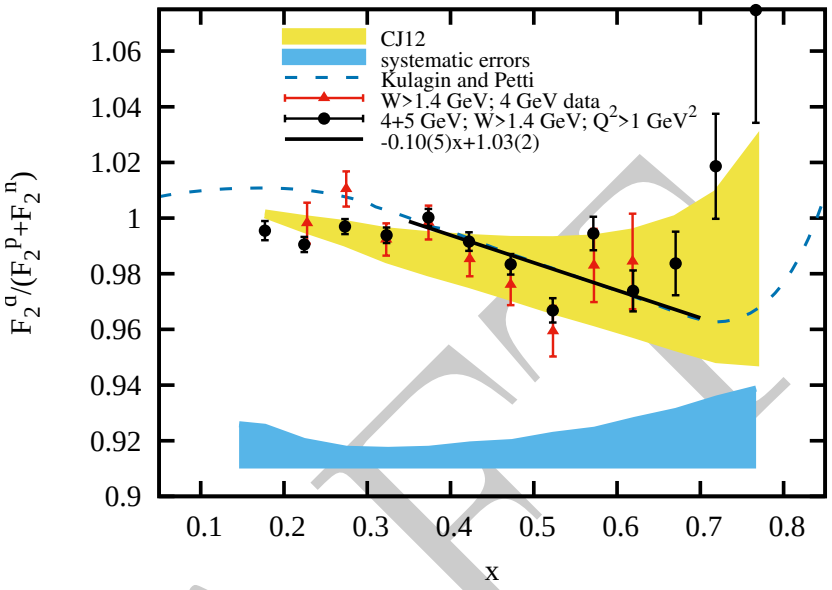

Figure 3: $F_2^d/(F_2^n + F_2^p)$ ratio from the BoNuS experiment [24].

In addition to extracting the free neutron structure function from tagged measurements of the deuteron, we will also directly measure the proton and deuteron structure functions from the inclusive data on the proton and deuteron targets included in the TDIS proposal [25]. This will allow for a direct extraction of the "EMC effect" in the deuteron from $F_2^d/(F_2^p + F_2^n)$, as was done in the BoNuS experiments [24], as shown in Fig. 3. Note that they obtain a slope of 0.1 ± 0.05, while a recent analysis attempting to examine the universal EMC effect in the deuteron yields slopes of 0.05 vs 0.08 for different models of the underlying physics (off-shell effects vs. modification resulting from nucleon overlap) [26, 27]. Our statistics will be significantly better, allowing for an improved extraction of the slope as well as a comparison of the shape of the nuclear effects in the deuteron to the modification obtained from extrapolation of the EMC effect in heavier nuclei.

3.1.3 Resonance Region Structure Functions

While extensive measurements have been made in the resonance region for proton and deuteron targets, including recent measurements in Hall C [28], extraction of the F_2^n suffers from the same problems as in the DIS case - the need to remove the large proton contribution and the need to remove nuclear effects in the deuteron. For the resonance region, the impact of the Fermi motion is particularly important, as subtraction of the proton contribution is sensitive to the smearing applied to the proton structure function.

Figure 4 shows the extracted resonance region F_2^n from the BoNuS experiment [23]. For the most part, the resonance structure is clearly visible only at the lowest Q^2 or lowest W^2 values, and the statistics make it nearly impossible to isolate the resonance contribution from the non-resonant production. The TDIS-n measurements will significantly increase the kinematic coverage and statistics for the resonance region, as shown in Sec. 5.3.2.

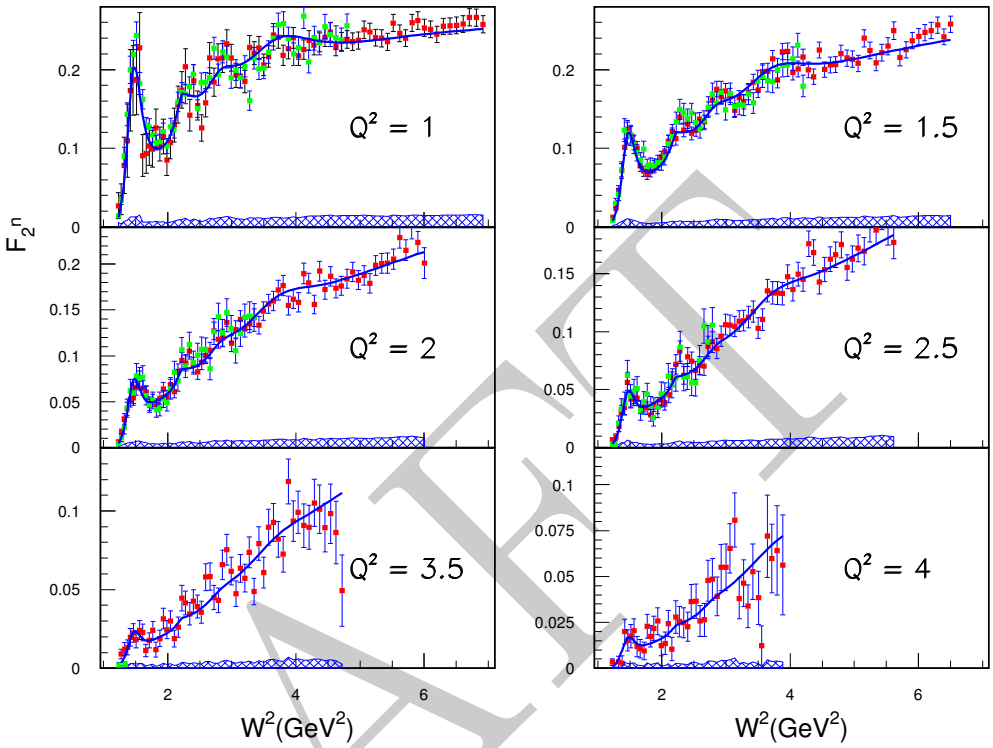

Figure 4: F_2^n in the resonance region from the BoNuS experiments [23] for several bins in Q^2. Different colors correspond to different beam energies. Error bars indicate statistical uncertainties only, while the blue bands at the bottom correspond to the systematic uncertainties for the highest energy point (5.3 GeV - red data points).

3.1.4 Elastic e-n Scattering

In addition to the structure function measurements, inclusive electron scattering from the tagged neutron will also allow for the extraction of elastic electron-neutron scattering. Figure 5 (left panel) shows the high-Q^2 measurements of G_{Mn}. Precision measurements are limited to $Q^2 < 5$ GeV^2 and come from only one measurement [3]. Additional measurements in this region, utilizing a different technique, will provide a cross check of the systematics associated with the neutron detection efficiency in the $d(e,e'n)/d(e,e'p)$ data, and can extend precision measurements to larger Q^2 values.

The right panel compares the elastic e-n peak from the BoNuS [23] to their simulated e-n elastic scattering cross section. While the tagged elastic events are in good agreement with the simulation, the limited statistics did not allow for a meaningful extraction of the neutron magnetic form factor. The higher TDIS-n beam energy, luminosity, and detector rate capability will provide elastic measurements with significantly higher statistics, allowing for an extraction of G_{Mn} up to modest Q^2 values.

3.2 Spectator Tagging Formalism

Energy conservation requires that the deuterium mass be the sum of the proton and the neutron energies: $E_p + E_n = M_d$. Because the mass of the deuteron is smaller than the mass of the proton plus the neutron, one or both nucleons must be off-shell. For certain kinematics, we can assume that the proton is a spectator and on-shell, while the neutron is off-shell with an $E^* = M_d - \sqrt{M_s^2 + p_s^2}$.

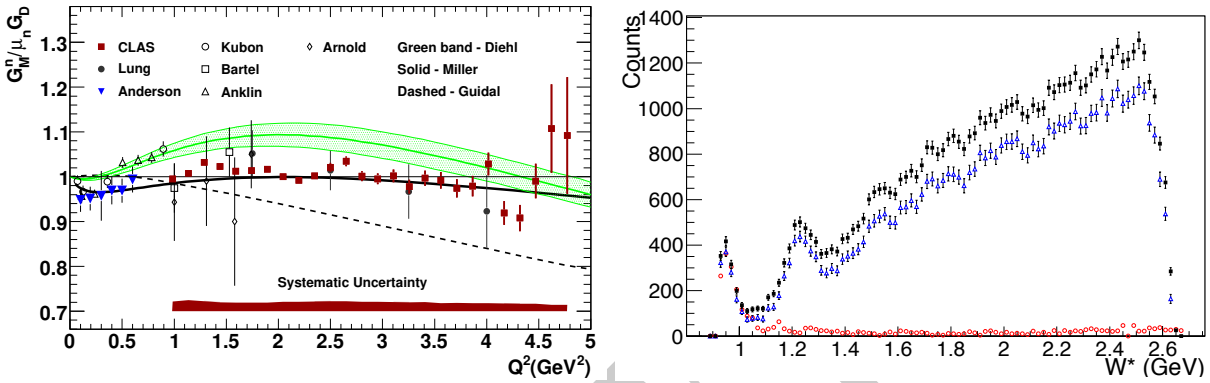

Figure 5: (Left) High-Q^2 extractions of the neutron magnetic form factor, G_{Mn}, taken from Ref [3]. (Right) The W^* distribution for Q^2 from 1.1 to 2.23 $(\mathrm{GeV}/c)^2$ from BoNuS [23]. Black and blue points are data before and after subtraction of accidental coincidences, and the red points are the simulated yield for the elastic peak, including radiative tail, indicating that the tagged elastic peak is well reproduced.

The final state motion of the spectator nucleon can be described by the light-cone fraction α_s:

$$\alpha_s = \frac{E_s - p_{s\parallel}}{M_s} . \tag{5}$$

In the plane wave impulse approximation (PWIA) the recoiling proton momentum is equal and opposite to the neutron, thus the 4-momentum of the off-shell neutron is $p_n^\mu = (M_d - E_s, -\vec{p}_s)$, with M_d the mass of the deuterium nucleus. In the PWIA, the neutron is assumed to be on the energy shell, but off its mass shell, therefore the invariant mass of the free nucleon is:

$$M^{*2} = (M_d - E_s)^2 - \vec{p_s}^{\,2} . \tag{6}$$

In the same way, the Bjorken scaling variable $x = \frac{Q^2}{2M\nu}$ is replaced by:

$$x^* = \frac{Q^2}{2p_n^\mu q_\mu} = \frac{Q^2}{2\left((M_d - E_s)\nu + \vec{p}_s\vec{q}\right)} . \tag{7}$$

Assuming $M_d \approx 2M$, $\vec{p}_s\vec{q} = p_{s\parallel}|\vec{q}|$, in the Bjorken limit $|\vec{q}|/\nu \to 1$, the light-cone fraction α_s, Equation 7 becomes:

$$x^* = \frac{Q^2}{2M\nu\left(2 - \frac{E_s - p_{s\parallel}(|\vec{q}|/\nu)}{M}\right)} \approx \frac{Q^2}{2M\nu(2-\alpha_s)} = \frac{x}{2-\alpha_s} . \tag{8}$$

The total invariant mass of the hadronic final state in the $d(e,e'p_s)X$ reaction (see Figure 6):

$$\begin{aligned} W^{*2} &= (p_n^\mu + q^\mu)^2 = M^{*2} - Q^2 + 2(M_d - E_s)\nu + 2\vec{p}_s\vec{q} \\ &= M^{*2} - Q^2 + 2M\nu\left(2 - \frac{E_s - p_{s\parallel}(|\vec{q}|/\nu)}{M}\right) \\ &\approx M^{*2} - Q^2 + 2M\nu(2-\alpha_s) . \end{aligned} \tag{9}$$

The differential cross section with kinematics defined by the spectator-model values α_s and p_T can be calculated as:

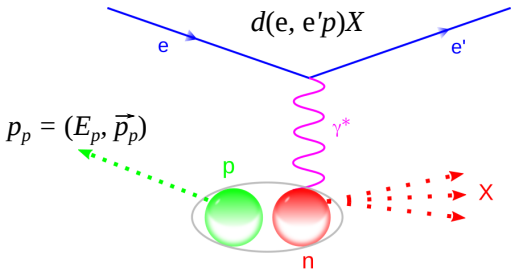

Figure 6: Diagram of the $d(e,e'p)X$ process. A high energy electron interacts with a deuterium nucleus through a virtual photon. The recoil proton is detected, ensuring that the virtual photon struck the neutron.

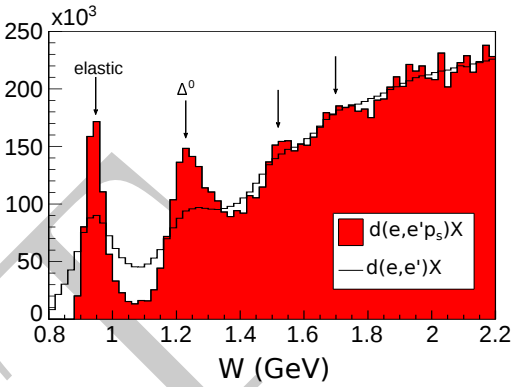

Figure 7: Invariant total mass spectra from inclusive scattering on deuterium compared (black line) with the tagged spectra (red area) showing the advantage of the method making the resonances to stand out. From [14] and N. Baillie PhD Thesis, W&M (2010).

$$\frac{d\sigma}{dx^* dQ^2} = \frac{4\pi\alpha_{EM}^2}{x^* Q^4}\left[\frac{y^2}{2(1+R)} + (1-y^*) + \frac{M^{*2}x^{*2}y^2}{Q^2}\frac{1-R}{1+R}\right] \times F_2(x^*, \alpha_s, p_T, Q^2)\, S(\alpha_s, p_T)\frac{d\alpha_s}{\alpha_s} d^2p_T \tag{10}$$

in which $S(\alpha_s, p_T)\frac{d\alpha_s}{\alpha_s}d^2p_T$ is the probability of finding the spectator at p_T and α_s with the given kinematics, $R = \frac{\sigma_L}{\sigma_T}$ is the longitudinal to transverse cross section ratio, $y = \nu/E$ and $F_2(x^*, \alpha_s, p_T, Q^2)$ is the off-shell structure function of the struck neutron. Therefore $F_2^n = F_2(x^*, \alpha_s, p_T, Q^2) = F_2^{n\,\mathrm{free}}(x, Q^2)$. Further details are given in Refs. [22, 29].

The tagging method was used in BoNuS at Hall B at JLab in 2005 [14, 23], and recently in BoNuS12 at JLab in 2019 (under analysis). An example of the advantage of the method is presented in Fig. 7 showing the total invariant mass spectrum comparing the untagged spectra with the spectator tagged method. It is evident how the elastic and Δ^0 peaks improve their resolution and how the resonances stand out more clearly.

3.3 Model-dependent Corrections in Extracting the Free Neutron Structure

The spectator tagging method needs to accomplish several kinematics conditions in order to be considered useful as a free neutron measurement. The off-shell effects (the difference between the free neutron SF and the effective SF) were studied by different theory groups [30, 20, 21], showing that selecting a very low momentum recoil proton, yields small corrections from the ratio $R_n \equiv F_2^{n(\mathrm{eff})}/F_2^n$. Figure 8 shows the calculated off-shell effects for two different models. Below 200 MeV/c, the calculations show a reduction in the effective neutron SF below ∼5% [30] and 2% [20, 21], while below 100 MeV/c, the corrections for the two calculations are below 2% and 1%, respectively.

Another possible source of uncertainty is the final-state interaction (FSI), where the spectator proton interacts with deep inelastic remnants of the struck neutron. Several groups have calculated FSIs, demonstrating that backward-going spectators minimize such effect [31] (figure 9).

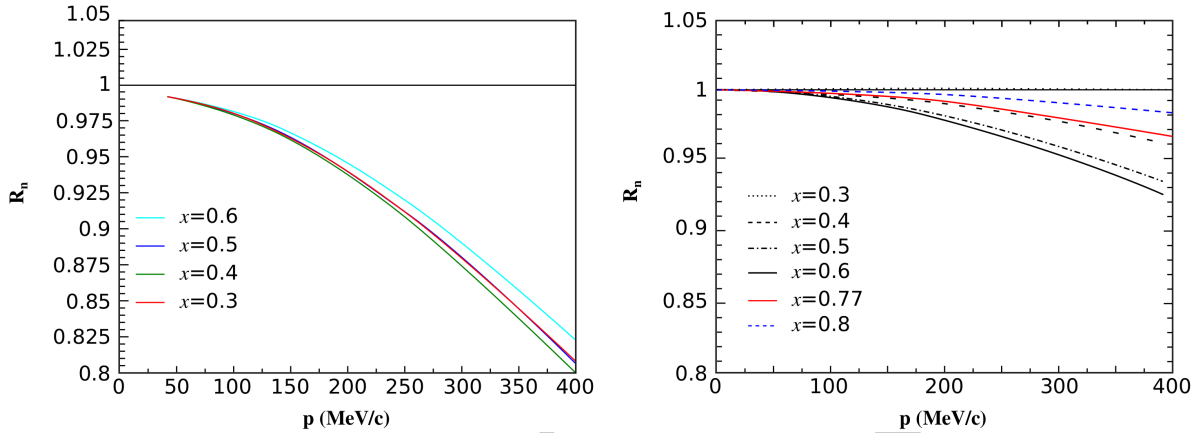

Figure 8: Off-shell effect dependence vs proton recoil momentum for different x values. The left panel shows the off-shell effects from [30], while the right panel shows the model from [20, 21].

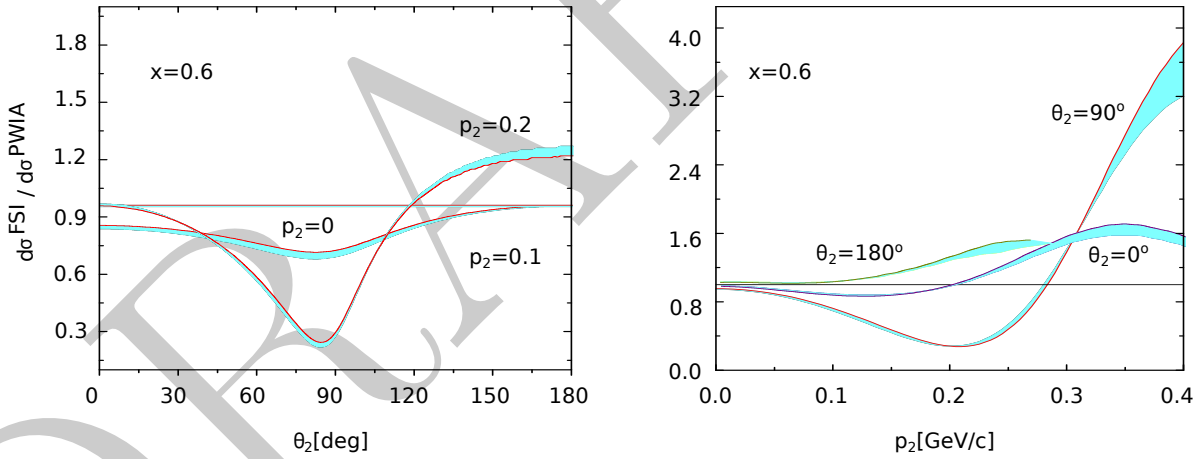

Figure 9: Final-state interaction model from [31]. **Left**, The FSI, PWIA ratio vs spectator proton angle for three different momenta (in GeV/c) at $x = 0.6$,. It shows that at very backward emission angles, the ratio difference from unity is practically negligible for protons at 100 MeV/c and $\sim 20\%$ for 200 MeV/c protons. **Right**, FSI, PWIA ratio vs spectator proton momentum for three different emission angles at $x = 0.6$. It shows that the effect is reduced for low spectator proton momentum and specially at high backward angles.

To minimize the impact and uncertainty of off-shell effects and final-state interactions, we use the tagger to select events where the proton momentum is low and $\theta_2 = \theta_{pq}$ is large. For the projections included below we take only events with spectator proton momentum from 60-100 MeV/c and for $\theta_{pq} > 100°$. This is nearly identical to the cuts used in the BoNuS analysis [14], except that their lower limit for recoil momentum was taken to be 70 MeV/c, while based on the studies of the mTPC efficiency (as shown in in Fig. 14) show good acceptance down to 60 MeV/c.

Because of the high statistics, especially in the modest x region, we can examine the yields as a function of momentum cut applied to the proton spectators. With a factor of 7 times more statistics than the BoNuS12

proposal for our kinematics 7, we can divide the data into three bins of spectator momentum to verify that the corrections are consistent with the models presented in Figs. 8 and 9, with each bin giving roughly twice the statistics of the BoNuS12 measurement.

4 Experimental setup

As stated previously, we propose to use the TDIS setup with no other modifications. This section is dedicated to the description of the TDIS setup. The Super BigBite Spectrometer (SBS) will be used for measuring the scattered electron and a dedicated recoil detector, immediately surrounding the target, will be used to measure the spectator protons in coincidence. This setup is only briefly summarised below and a more extensive description is available in the TDIS proposal [25].

4.1 Scattered Electron Arm: Super Big Bite Spectrometer

The Super BigBite Spectrometer (SBS) is a ~ 30 msr acceptance spectrometer, composed of a single dipole magnet and a modular detector package. It is mainly (but not exclusively) dedicated to Form Factor measurements at high Q^2 ([32, 33, 34]). In these experiments (and others such as SIDIS [35]), SBS will be used as the "hadron arm", to detect the hadronic final state (recoil nucleon), and is being instrumented accordingly, e.g.: a hadronic calorimeter, and additional detectors: "CDet" hodoscope (G_M^n), GEM equipped focal plane polarimeter (G_E^p), etc.. SIDIS requires an additional RICH detector for hadron identification, and 5 planes of GEM trackers, each made of four modules of 60×50 cm^2, arranged to form 60×200 cm^2 trackers. TDIS will be one of the very few SBS experiments using it in "electron mode", which requires a slightly different detector package. This detector package includes most of the SBS detector package for SIDIS (including GEM trackers and RICH), but substituting the hadronic calorimeter for one module of the CLAS Large Angle Calorimeter (LAC), and modifying the RICH for electron/pion separation. The following three sub subsections describe the detector systems that are specific to SBS in electron mode. Please note that these modifications are already necessary for TDIS and preparations of the modifications are underway by the TDIS collaboration.

GEM Chambers To perform the tracking of charged particles under the high rates anticipated for SBS experiments, drift chambers have been in general replaced with gas electron multiplier (GEM) detectors.

These detectors have proven to be capable of operating under luminosities of 25 kHz/mm^2 for the COMPASS experiment at CERN and the spatial resolution of each of these chambers is anticipated to be about 70 μm. There will be five layers of GEMs composed of four modules measuring 50 $\times$ 60 cm^2 , such that the layer covers 60 $\times$ 200 cm^2, the long dimension being along the dispersive direction of the SBS spectrometer. The readout of these modules are all oriented in the x/y direction. Fig. 10 displays a single back GEM layer.

For two sets of GEM chambers separated by a distance z_{GEM} and including multiple scattering effects, the angular resolution can be approximated by

$$(\delta\theta)^2 = \frac{\sigma_x^2}{z_{\mathrm{GEM}}^2} + \left(\frac{13.6\ \mathrm{MeV}}{\beta cp}\sqrt{x/X_0}\,[1+0.038\ln(x/X_0)]\right)^2 , \tag{11}$$

where βc is the velocity of the electron, p is the momentum of the electron, and x/X_0 is the thickness of the scattering material in radiation lengths.

For small deflection angles from a dipole magnet, the deflection angle, θ, and the momentum, p, are related by the equation

$$p = \frac{e\int B_\perp \cdot dl}{\theta}, \tag{12}$$

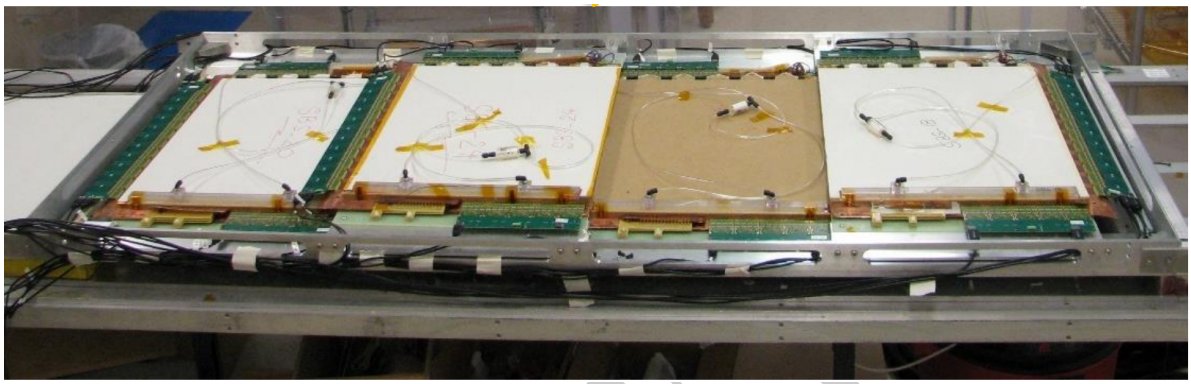

Figure 10: Picture of the back layer of GEMs, illustrating its arrangement

where $\int B_\perp \cdot dl$ is the field integral for the path of the electron. For electrons of momentum $3 \sim 4$ GeV and a field integral of 1.0 T $\cdot$ m, this would yield a typical momentum resolution of $\delta p/p \approx 0.5\%$.

CLAS6 Large Acceptance Calorimeter The conceptual drawing of the internal structure of the LAC is shown in Fig. 11. The LAC module has a rectangular shape with a sensitive area of 217 x 400 cm^2 and consists of 33 layers, each composed of a 0.20 cm thick lead foil and 1.5 cm thick NE110A plastic scintillator bars. The total thickness is about 12.9 radiation lengths or 1 hadronic absorption length. Each scintillator layer is protected from contact with the lead by 0.02 cm thick Teflon foils. The width of the scintillators is roughly 10 cm and is slightly increasing from the inner layers toward the outer layers to provide a focusing geometry. Scintillators in consecutive layers are rotated by 90 degrees to form a 40 x 24 matrix of cells with area approximately 10 x 10 cm^2. The module is vertically divided into two groups: inner (first 17 layers) and outer (16 layers) groups. Each group has its own light readouts. Scintillators lying one on top of the other with the same orientation form a stack. For each stack the light is collected at both ends separately using light guides coupled to EMI 9954A photomultiplier tubes. For each module there are 128 stacks and 256 photomultipliers [36].

The LAC energy resolution for electromagnetic showers is 7.5$\pm$0.2% [36]. Combined with CLAS, the pion contamination was less than 1% for cuts that give a detection efficiency of 95% for 2 GeV electrons.

The expected performance of this equipment for pion rejection has been evaluated with Monte Carlo for the TDIS proposal, and one may refer to [25] for more details about this matter.

Ring Imaging Cherenkov The RICH (Ring Imaging CHerenkov) detector has been recovered from the HERMES experiment at DESY [37]. Its original purpose (which will be the same for SIDIS) was to identify pions, kaons and protons, over a wide momentum range (to 12 GeV/c or above from $\sim$0.5 GeV/c for π/K, and from $\sim$2 GeV/c for K/p), from the reconstructed Cherenkov rings generated while the particles go through the radiator media. The RICH bears two Cherenkov radiators: an array of aerogel tiles ($n = 1.03$) covering the RICH aperture, for identification at lower particle momentum, and a heavy radiator gas (C_4F_{10}, $n = 1.00137$), for identification at higher momentum. The Cherenkov light rings are reflected by a spherical mirror to a large array of 1938 2.5 cm diameter XP1911 PMTs (see Fig. 12).

In TDIS, the RICH will be modified to a threshold configuration for the purpose of electron identification and pion rejection. First, the aerogel tiles can be removed entirely to suppress any low momentum signal apart from electrons. Second, the radiator gas, C_4F_{10} has to be substituted for lighter gas with a lower index of refraction (e.g. CO_2, CF_4), which increases even further the pion threshold, while still providing a sufficient

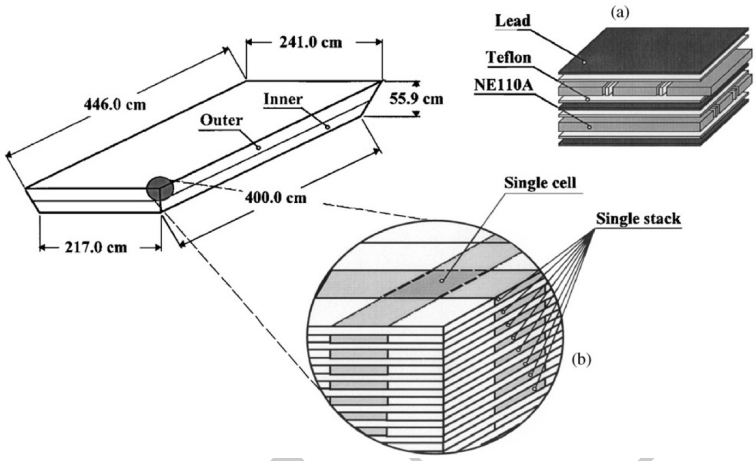

Figure 11: The conceptual drawing of the internal structure of the LAC module.

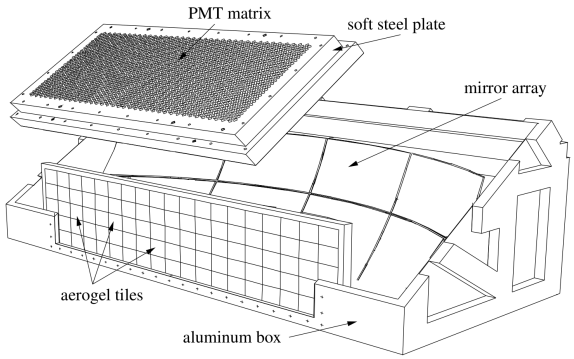

Figure 12: The HERMES RICH detector [37]. In electron mode, the aerogel tiles will be removed; the gas might also be substituted for lighter gas.

signal for the RICH. Simulations are have been performed and are on-going by the TDIS collaboration to optimise the gas settings for the RICH detector in threshold mode.

4.2 Recoil Detector: multiple Time Projection Chamber (mTPC)

Based on extensive simulation studies by the TDIS collaboration, the design of the recoil detector for TDIS has been updated significantly since the original pion and kaon TDIS proposals [25, 38], where a radial Time Projection Chamber (rTPC) was originally envisaged (similar to that used by BoNuS and BoNuS12). The novel mTPC ("multiple Time Projection Chamber") has primarily been re-designed to be high-rate capable and to operate at room temperature (the original rTPC was planned to be cryogenic). It is also much simpler than the rTPC in it's design and construction, since the GEM-based readout system will be planar rather than cylindrical in shape. It's design is described further below.

The mTPC is a 50 cm long time projection chamber with a cylindrical geometry, centered on and surrounding the 40 cm target and positioned within the bore of the 4.7 T solenoid of the TDIS setup. The

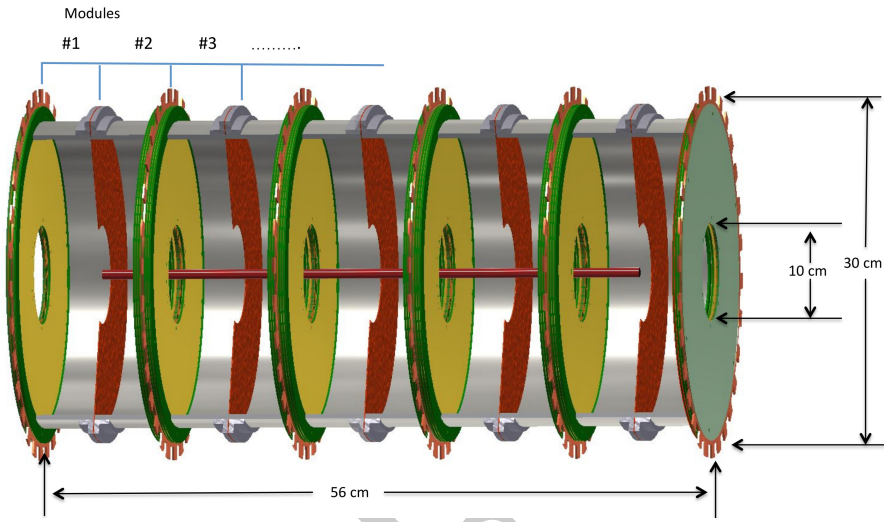

Figure 13: mTPC current design. The mTPC is segmented into chambers longitudinally along the beam line to deal with high rates. There are 10 chambers, of 5 cm length each, to minimize the drift time in each module and allow for a faster detector response. The yellow disks are the readout planes (which consist of GEM foils) and the red disks are the HV planes which are used to setup the electric field parallel to the beam line direction for drifting the ionisation created by traversing hadrons towards the readout planes with as short a drift path length as possible.

mTPC active volume has an inner radius of 5 cm and an outer radius of 15 cm. Its purpose is the detection of the low energy spectator protons (and decay protons and pions) for the pion (and kaon) TDIS measurements, and the spectator proton in the TDIS-n measurement on deuterium. These hadrons all lie within the range of 60 to 400 MeV/c. Fig 13 shows a CAD model of this detector from the TDIS collaboration.

The mTPC's main feature is its longitudinal segmentation, which is capital provided the experiment luminosity and background. Extensive Monte-Carlo simulation work carried out by the TDIS collaboration within the SBS Collaboration's GEANT-4 simulation framework (G4SBS) has indicated that the background rates at the mTPC detector location will be significantly higher than the rates handled in similar size TPCs before. Dividing the detector longitudinally, however, primarily reduces significantly the background received in each chamber by a factor 10, to levels which have been deemed acceptable by the TDIS collaboration. The segmentation also allows to minimize the drift time of the ionisation caused by traversing hadrons to the order of a couple of μs, due to shorter drift distances and simpler electric field setup compared to the original rTPC design (reduction by a factor 20-40). Furthermore, the new planar GEM readout design should also be simpler to construct than the more complex cylindrical shapes.

As explained in Fig. 14, the drift electrons from the ionizing particles will be amplified and detected by GEM foil based readout disks. The readout disks (yellow disks in Fig 13) each consist of two GEM layers, each mounted on a 2 mm thick holding frame, followed by a readout surface containing conducting pads connected to readout electronics through traces on the back of the readout and then through a flex circuit strip. Each readout pad is currently planned to have an area of 5 x 5 mm^2 separated by gaps of 100 μm, yielding approximately 2500 pads per readout. This arrangement gives position resolution of approximately 1.5 mm. The drift gas will be composed of 70% ^{4}He and 30% CH_4 held at room temperature. This choice is dictated by the necessity to have a low Z material to minimize the number of secondaries created in the gas and minimise multiple scattering. The expected drifting and diffusion of ionisation in the mTPC and the readout GEMs has been verified through Magboltz and Garfield++ simulations by the TDIS collaboration.

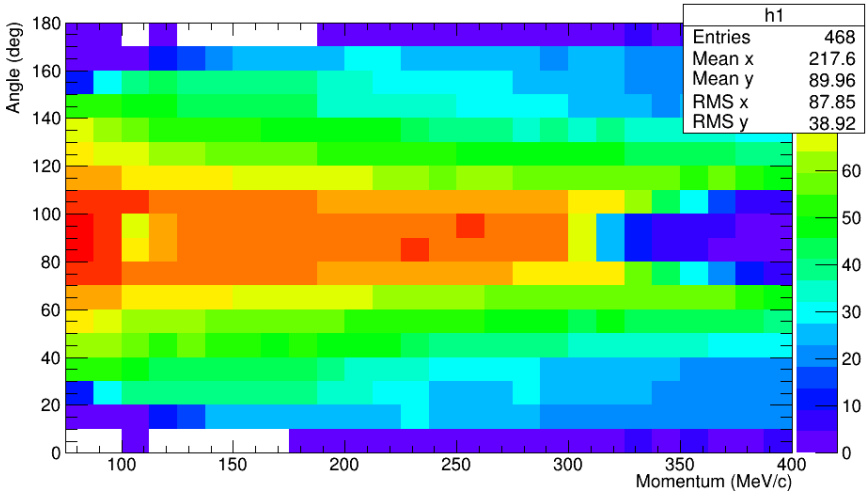

Figure 14: mTPC efficiency.

As explained, the modular design is key for the mTPC to handle high background rates, however this is at the cost of reduced efficiency and reduced momentum resolution due to the presence of readout disks in the middle of the active area which reduce the track lengths in the drift volume. For mTPC studies which have been performed, any track reconstructed in the mTPC with a momentum uncertainty of over 10% is rejected, leading to decreased efficiency. This is our current definition of mTPC efficiency for the TDIS experiments. A semi-empirical map of the mTPC efficiency as a function of the proton momentum and angle (with respect to the beam direction, not the same as θ_{pq}) is shown in Fig 14. The efficiency lies in the range of 50% to 70% for detecting proton tracks with momenta in the range of 70 MeV/c to 300 MeV/c with a transverse momentum resolution of 10% or better. Simulations have demonstrated tagging below 70 MeV/c in the past and these have to be updated. For our studies, for 60 – 100 MeV/c we have taken the average efficiency to be 50% and if we take a minimum momentum of 70 MeV/c, the loss in statistics is $\sim$ 30%. TDIS collaboration will continue to investigate optimization of detection of low momentum recoil protons down to 60 MeV/c. For tracks in the momentum range of 300 MeV/c to 400 MeV/c, this efficiency is higher than 20%. Note that the mTPC has azimuthal symmetry with the current simulated geometry, so there is no ϕ dependence on the efficiency. These anticipated inefficiencies are sufficient to meet the physics goals of the TDIS program.

4.2.1 mTPC Readout and Streaming DAQ Developments

The mTPC will require a high rate capable readout system. Currently the TDIS Collaboration are investigating and prototyping a small-scale readout system based on the SAMPA ASIC incorporated on front end cards. The original design of the SAMPA-based readout system was developed for and used in the upgrade of the ALICE TPC for the high luminosity upgrade at CERN [39, 40]. The SAMPA ASIC is extremely interesting for such a high rate application as the TDIS and its related run group experiments, as it provides the capability to operate the readout electronics in triggered or streaming (continuous readout) mode. A full description of these developments made so far by the TDIS collaboration may be found in [41] - in which the general design of the front end electronics are described, as well as preliminary results from a small-scale streaming DAQ prototype of the electronics connected to a GEM detector which is used to measure cosmic

ray data.

Our experiment will not require any modifications to the proposed readout system for the mTPC, and on-going developments by the TDIS collaboration will be directly relevant and beneficial to this measurement also. The development of streaming readout electronics for these measurements may also be of significant interest to any future experiments which also propose to use high rate capable DAQ systems for the readout of GEM detectors (e.g. SoLID).

4.3 Target and Expected Luminosity

Our proposed measurement will use the same target as the TDIS experiment. The design of this target has also been upgraded since the original TDIS proposal and the TDIS Collaboration is also currently prototyping the novel target design and production processes. The main motivation for the target design change was to move from a cryogenic target to a room temperature one.

Since the thickness of the target walls and gas material are crucial due to the low momenta of the hadrons to be measured in the mTPC, the momentum threshold for hadrons escaping the new target configuration has been fully modelled by the TDIS Collaboration in the G4SBS simulation package (described in section 5.1) - studying several target wall thicknesses and gas pressures. Testing the manufacture of different wall thicknesses with materials available from manufacturers (which align with the thicknesses required from the simulations), and testing of the resulting target structures under pressure are currently underway by the TDIS collaboration.

The current design of the TDIS target as a result of these studies is a 40 cm long, 1 cm diameter straw filled with gaseous deuterium (or hydrogen), at 6.4×10^{-4} g/cm^{-3}. In order to minimize the energy loss of the protons of interest, we have reduced the material of the target wall as much as possible, down to 20 micrometers of Kapton. To achieve the target density, the gas will be held at room temperature and $\sim$4 atm. The choice will ultimately depend on the pressure the walls are able to handle (or by how much they need to be thickened). Combined with the beam intensity, this will be capable of providing us an instant luminosity per nucleon of 2.9×10^{36} cm^{-2}s^{-1}.

The proposed measurement concerns a process with a relatively low cross section (typically fractions of nb), which requires a relatively high luminosity and/or wide acceptance to collect a significant statistics. In addition to this, the detection efficiency of the very low momentum spectator proton will provide a significant reduction of the available statistics. Besides, the spectator tagging technique requires a relatively low density target to reduce the detection threshold of the spectator, which limits the intensity.

4.4 Trigger

The experimental trigger is based on the combination of the LAC and the RICH information. To trigger on the electrons of interest, a minimum energy deposit in the LAC, equivalent to the energy deposit a 1.0 GeV electron, is required. To reject pions, the LAC longitudinal segmentation is also exploited: it is required that the energy deposited in the "inner" layer of the LAC has to be at least 25% of the energy deposit of the outer layer. For photon rejection (and further charged pion rejection), the electromagnetic cluster in the LAC has to be associated with a significant signal in the RICH: at least 3 PMTs have to be fired in a region of the RICH matching the position of the electromagnetic cluster in the LAC. Simulations of the trigger rate give estimates of 6 kHz in the SBS, estimated from well-known inclusive electron scattering at somewhat small angle.

Beam on target rates in LAC scintillators have been evaluated for n-DVCS with TDIS. These studies show that the backgrounds in the LAC should not significantly contribute to the trigger rates.

4.5 Expected Backgrounds

The expected background rates for this measurement will match those for the TDIS measurements due to the identical running conditions and no new configuration requests. A more thorough explanation of the expected background rates and processes may be found in the TDIS proposals [25, 38]. The hydrogen background numbers below are taken from the TDIS proposals. Since the proposals, the TDIS collaboration has re-visited the background projections for the deuterium target case and those latest numbers are given below. These numbers are slightly lower than those reported in the proposals (which may therefore be considered a worst case scenario).

For hydrogen target running the background rates are quoted for a proton angular range of $30° < \theta_p < 70°$ with respect to the beam direction, as provided in the TDIS proposals due to the predicted range of coverage for TDIS events in the recoil detector. Elastic scattering cuts can remove the very high expected rate of low momentum protons arising from e - p scattering (170 MHz), which predominantly scatter in the range 78 - 88 °. This will be achievable since the mTPC has the capability to resolve the polar angle between the hadrons and the beam direction. The resulting rate from this process in the $30° < \theta_p < 70°$ range is 0.2 MHz. Photoproduction will lead to a higher rate of ∼10 MHz in this angular coverage. The upgrade of the recoil detector to the current mTPC design, will result in a reduction of this expected rate to ∼1 MHz per chamber, also reducing the probability of protons to be accidentally detected in coincidence with the DIS electron by a factor of ten compared to the original TDIS proposal (0.01 per electron originally [25]).

For the deuterium target, recent studies, making use of the epc.f code [42] show that single proton rates with maximum momentum of 1.2 GeV/c are on the order of 123 MHz in the location of the mTPC. DIS background mainly arise from charged pions and, in small numbers, protons. Making use of pre-generated minimum-bias PYTHIA events[4], it is possible to set a maximum expected background rate from DIS without any considerations of geometry, except the space where the particles are generated (the drift region of the mTPC). PYTHIA data have been simulated as *ep* and *en* scattering events in a fixed target with a constant electron beam energy of 11 GeV, without any explicit limits to Q^2 or W^2. Resulting particle rates for the proton target are: π^+ 730 kHz, π^- 590 kHz, p 150 kHz. For the neutron target they are: π^+ 430 kHz, π^- 690 kHz, p 86 kHz.

5 Projected Results

5.1 Event Generator

We have used two simulations to estimate the counting rates for this experiment. The first is G4SBS [43], a Geant4 based detailed simulation of the SBS detector, used for rate, trigger, and background studies. The second is a separate fast simulation using only geometric acceptance and an effective free neutron target which allows for the inclusion of various more detailed cross section models for modest-Q^2 values and resonance region production, and which provides free neutron spectra with resolution applied to approximate the neutron spectra from the spectator-corrected e-n scattering.

The G4SBS simulation package: G4SBS is a Geant4 based Monte-Carlo simulation package developed by the SBS collaboration to evaluate the response of the SBS detectors to different physics channels. G4SBS includes a detailed description of each of the detectors, and can be configured for each of the SBS experiments, including TDIS. Fig 15 shows a visualisation of G4SBS in the TDIS configuration. The magnetic fields can also be configured to include the solenoid field in the target region as well as the SBS magnetic field. G4SBS also includes a wide array of physics generators.

[4] A. Puckett, internal communication

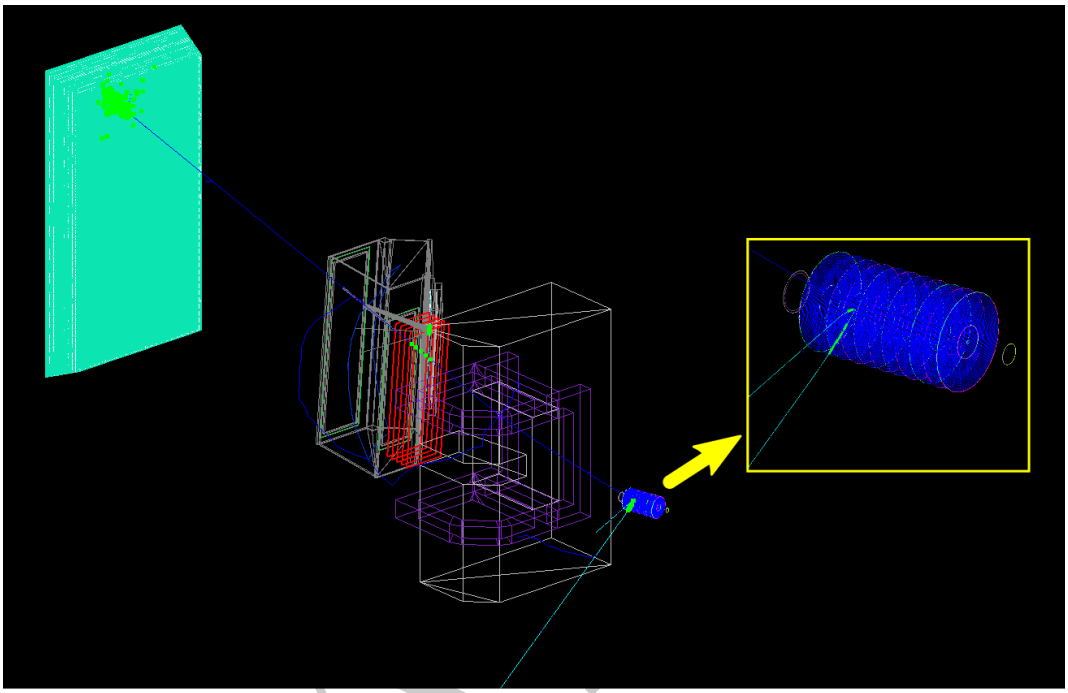

Figure 15: Screenshot of a Geant4 event simulation of the TDIS set-up. An electron scattered from the target (blue line) is detected within the SBS magnet and interacts with the GEM detectors, the GRINCH detector, and the LAC at the very end of the spectrometer. The produced recoil hadron (cyan line) is detected at the mTPC which surrounds the target. The yellow box shows a zoomed view of the simulated mTPC. Simulation by E. Fuchey and R. Montgomery

Fast simulation: A separate 'fast' simulation based on SIMC allows us to run a less complete but realistic high-statistics inclusive e-n simulation. This provides an approximation of the spectator-corrected inclusive results and allows us to easily modify the cross section model to optimize the simulation for the DIS and the modest-Q^2 resonance regions separately. Note that at this point the fast simulation is being used mainly for determining the yields, and does not yet incorporate realistic resolutions for the detector. This will mainly be relevant for the elastic and resonance region structure, and with anticipated resolution very similar to that of the BoNuS measurement, it should not significantly impact any of the physics extractions.

In the G4SBS simulation, we have used a deep inelastic scattering generator using the CTEQ6 [44] structure function parametrization. For this comparison, G4SBS simulated the proton tagging distribution and the mTPC efficiency and took a combined 2.5% efficiency to account for the combined mTPC and SBS efficiency, combined with the fraction of spectator protons passing the cuts (60-100 MeV/c momentum, $\theta_{pq} > 100$ degrees). For reference, this is consistent with the tagging efficiency and acceptance extracted for the BoNuS experiments [14], which looked at protons from 70-100 MeV/c), and is somewhat conservative compared to our projected efficiency. This cross section model does not include higher twist nor resonance structure, and is not suited to describe high x and modest Q^2 (*i.e.* lower W^2), as rates fall off too rapidly in this region.

We compared this simulation to a separate "fast" simulation using geometric cuts and an effective free neutron targets to allow us to run a high-statistics inclusive e-n simulation and easily change the cross section model. For the fast simulation, we modify the luminosity to account for a 10% chance of having a

spectator proton of 60-100 MeV/c with $\theta_{pq} > 100$ degrees, and take an average efficiency of 50% (mTPC + SBS), yielding 5% of e-n events from the deuteron yielding a spectator proton that passes our cuts. After correcting for the fraction of useful spectator protons and the tagging efficiency, we assume an 80% combined SBS efficiency and livetime for our projections for a 4% overall acceptance/efficiency correction.

The DIS rates in the fast simulation are ∼40% larger than for the full G4SBS simulation and in the region where the cross section models should be in good agreement, which is mainly explained by the different overall efficiency factor applied in the two simulations. At larger x, the fast simulation is still larger after correcting for this effect. This is mainly because the geometric acceptance cuts in the fast simulation yield slightly more acceptance at small scattering angle where the cross section is largest. While the total yield is therefore somewhat higher, the lowest angle data are not included in our projected results below, and in the region of interest, the simulations are in good agreement.

5.2 Kinematic Coverage

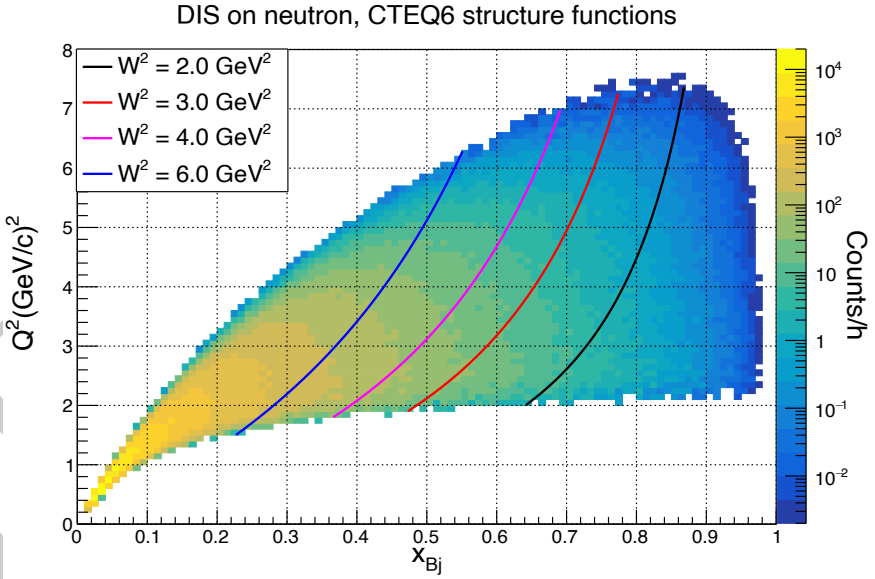

Figure 16: Q^2 vs x kinematic coverage for the SBS at 12 deg from the Geant4 simulation. The structure function parametrization from CTEQ6 [44] was used to calculate the DIS cross section for this Monte Carlo sample.

Fig 16 shows the kinematic coverage of the SBS spectrometer at 12 degrees away from the beam, in the TDIS configuration, based on the G4SBS simulation. The events in this Monte Carlo sample are weighed with a DIS cross section using the structure functions parametrization from CTEQ6 [44]. Because this does not include resonance region contributions, the comparison to the fast simulation results (Left panel of Fig 17) should only be made for $W^2 >$ 3-4 GeV^2. In addition, because the cross section does not include higher twist corrections nor resonance structure, the projections for the largest x (smallest W^2) regions are significantly underestimated.

Therefore, we use the fast simulation with a realistic model of the resonance region spectral function to estimate our expected statistics. As noted in the previous section, the fast simulation acceptance is too large for the smallest scattering angle, yielding additional statistics for $Q^2 < 2$ GeV^2, so exclude data below $Q^2 = 2$ GeV^2 in making our projections.

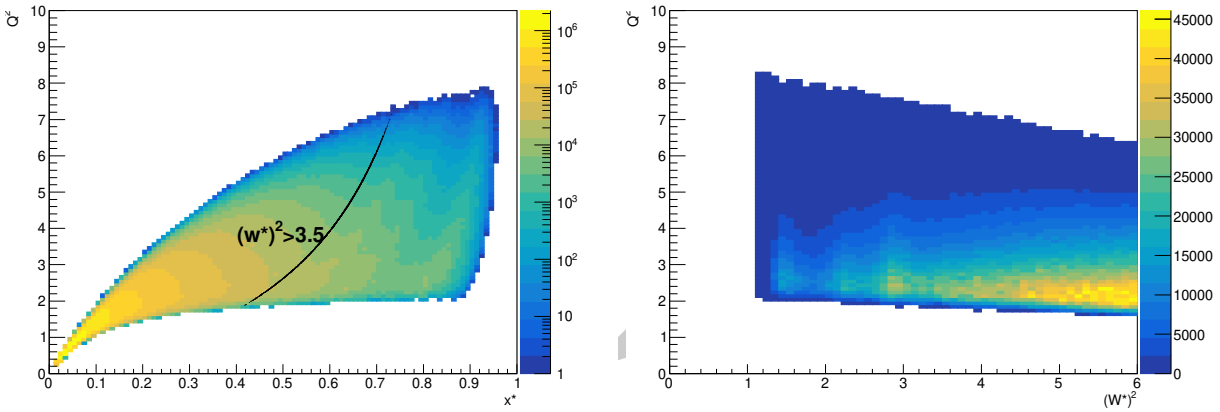

Figure 17: Q^{*2} vs x^* (left), and Q^{*2} vs W^{*2} (right) kinematic coverage for the SBS at 12 deg from a fast phase-space simulation. The * indicates that the neutron initial momentum has been corrected by tagging. The F1F209 model was used to calculate the inelastic neutron cross section, yielding a clear resonance structure and an increased cross section for the largest x and Q^2 values compared to the DIS model of Fig. 16. The colormap shows estimated counts with 5 days of beam.

The fast simulation was used to estimate the final statistics of tagged neutron events in the resonance region as shown in Figures 17 . The neutron cross section was calculate with F1F209 model [45]. Counts were estimated with luminosity of 1.5e36 deuterons/cm^2/sec and 5 days of beam. The fraction of spectator proton with initial momentum between 60 and 100 MeV and $\theta_{pq} > 100$ degrees is 9.9% based on Av18 calculations. A 50% average spectator detection efficiency for these protons, in addition to an 80% combined SBS efficiency and livetime.

5.3 Impact of the data

As noted in Section 3.1, tagging of spectator protons opens up inclusive measurements of e-n scattering over a wide kinematic range. We indicate below the kinematic coverage and projected statistics achievable for DIS scattering, resonance production region, and elastic scattering.

5.3.1 DIS data

Figure 6 shows the projected statistics for F_2^n and σ_n/σ_p for the 5 days of deuteron running. Note that while the statistics are large down to $x = 0.2$ and below, the radiative corrections and pion contamination become large, limiting our ability to make clean measurements at the lowest x values. However, a clean extraction of the structure function for 0.2-0.3 $< x <$ 0.7 with high statistics is achievable.

This provides a comparison of results for σ_n/σ_p with systematic uncertainties that are completely different from the MARATHON results [1]. In addition, it will provide tests of the tagging efficiency that are not possible in the BoNuS12 measurement, as described in Sec. 5.3.4. Finally, by looking at the extracted neutron cross section as a function of spectator proton momentum, we can test the models we rely on to show that the off-shell effects are small for our spectator proton cuts.

The region of $0.3 < x < 0.7$ is also of interest for examining the nuclear effects in the deuteron. The inclusive data from the TDIS measurement on proton and deuterium will provide inclusive measurements of F_2^p and F_2^d under experimental conditions very similar to the tagged F_2^n measurement, allowing for a

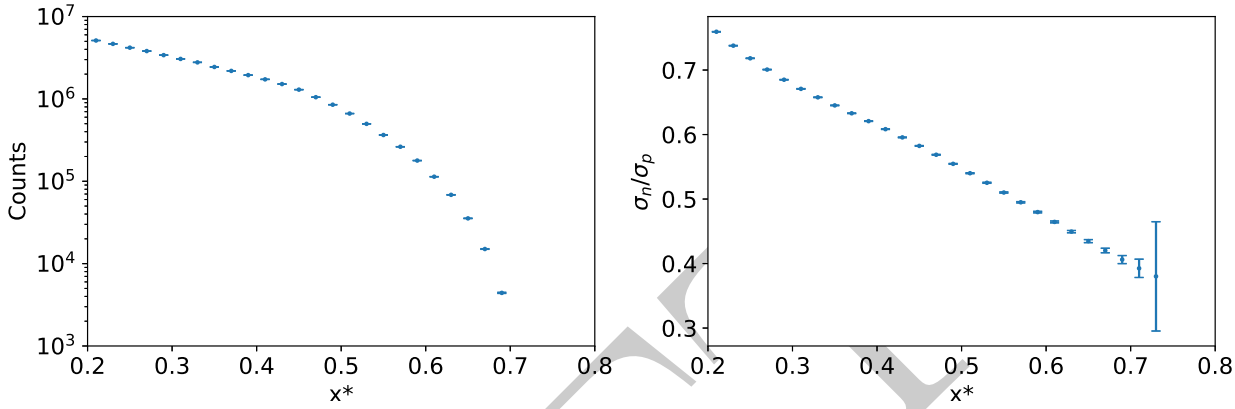

Figure 18: Projected statistics of tagged neutron events for F_2^n (left) and projected results for F_2^n/F_2^p (right) in the DIS region ($Q^2 > 1$ (GeV/c)^2, $W^2 > 3.5$ GeV^2) with 5 days of beamtime (statistical uncertainties only).

comparison of F_2^d to $F_2^p + F_2^n$, as shown in Ref. [24] and Fig. 3. Up to $x \approx 0.7$, we project a factor of 7 higher statistics than the projected BoNuS12 measurement [2].

5.3.2 Resonance region data

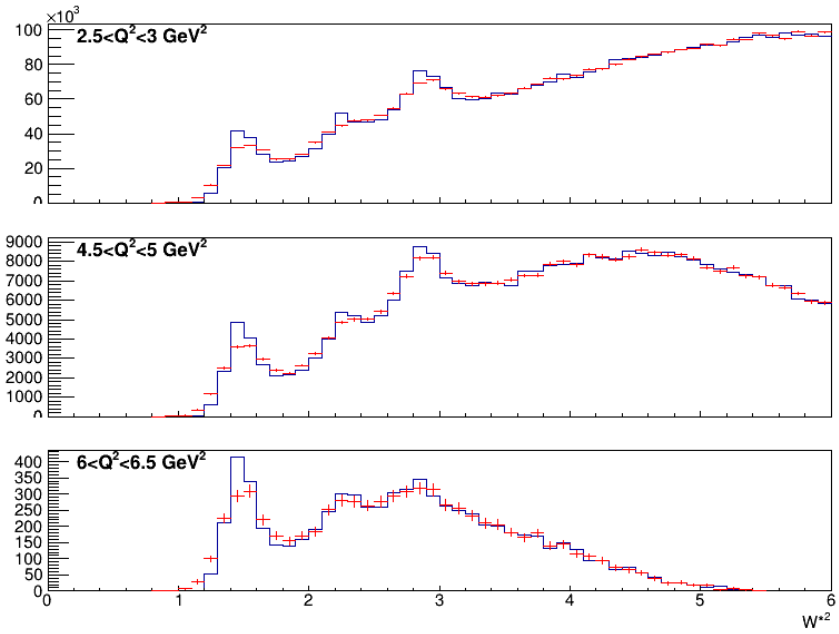

Figure 19: Estimated statistics of tagged neutron events in resonance region with 5 days of beam at various Q^2 range; spectra are with and without estimated resolution effects.

Figure 19 shows the projected F_2^n measurements as a function of W^{*2} for 3 bins in Q^2 to illustrate

the expected statistics of the measurement. This will provide a dramatic improvement on the BoNuS [23] extraction of F_2^n in the resonance region (as shown in Fig. 4 due to the higher beam energy and luminosity for TDIS-n. Our figure-of-merit is a factor of 7 higher than for the BoNuS12 measurement for the kinematics where they overlap, and for the larger Q^2 values of our measurement, the improved statistics will be important in studying resonance structure from the tagged neutron.

In addition to TDIS-n measurements of F_2^n, we will also analyze the proton and deuteron inclusive data to obtain F_2^p and F_2^d in the resonance region, with many common systematics that will allow for a better comparison of proton, neutron, and deuteron structure functions in the resonance region. With these data, we can compare the isospin structure of resonance electroproduction, in particular for the Δ to see if $\sigma_p \approx \sigma_n$, as expected for isovector transitions, or if there is evidence for isotensor contributions as seen in existing measurements comparing Δ electroproduction from the proton and deuteron [46].

High-statistics measurements of F_2^n in the resonance will also allow for additional checks of duality in the neutron, without relying on model-dependent extractions of the neutron resonance structure from the deuteron [47, 48, 49, 50] and with significantly higher statistics and improved Q^2 coverage compared to Ref. [51]. While our internal comparison of F_2^n in the resonance region to the DIS will be limited to lower x (and thus lower Q^2 or higher W^2), we can also compare our F_2^n/F_2^p in the resonance region to extractions of F_2^n/F_2^p in the DIS region from MARATHON or BoNuS12. This allows us to take advantage of the cancellation between systematic uncertainties in our neutron-to-proton ratio, and compare to reliable DIS measurements which can do the same.

5.3.3 Elastic e-n scattering data

The TDIS-n data will provide high statistics measurements of the elastic e-n cross section up to $Q^2 \approx$?? GeV^2, with very different systematics than the existing CLAS extraction from $d(e,e'n)/d(e,e'p)$. Taking the elastic data and splitting it up into bins of ΔQ^2=0.5 GeV^2, we project $\sim$1k events for Q^2 = 7 GeV^2, and >2k counts for Q^2 up to 6 GeV^2. This will provide high-precision overlap with the CLAS data shown in Fig 5 from 2-5 GeV^2, while also providing overlap with proposed 12 GeV measurements that go from Q^2=3 GeV^2 to $\sim$16 GeV^2. As this is the only measurement using spectator tagging, this will provide good cross checks of both data sets with completely different systematic uncertainties.

5.3.4 Tagging efficiency studies

The TDIS-n measurements have multiple ways to calibrate the tagging efficiency, which were not available for the BoNuS or BoNuS12 measurements [23, 2]. Those measurements determined bye overall tagging efficiency by normalizing the extracted value of F_2^n/F_2^p at $x \approx 0.3$ against extractions from the deuteron. Because they normalize their main observable against previous measurements, they build in any model dependence from the deuteron extractions at $x = 0.3$, and the BoNuS extractions of F_2^n/F_2^p for $x \approx 0.3$ are not truly independent measurement. While not using tagging methods, MARATHON makes a similar normalization of their ^{3}H/^{3}He cross section ratio [1].

TDIS-n can perform the same normalization, but we have two additional ways to determine the tagging efficiency. First, we can normalize based on the elastic e-n cross section measurements at low-to-modest Q^2, where the cross sections are relatively well known. This provides a cross-check of the normalization factor and allows the tagging efficiency to be determined from a physics measurement that is independent of F_2^n, the main observable of the measurement.

In addition, the 4.4 GeV data taking with the SBS hadron calorimeter (HCAL) configured to detect elastic e-n scattering provides, for the first time, a kinematically over-determined measurement allowing us to reconstruct the spectator proton momentum using only the SBS and HCAL measurement, allowing for a direct measurement of the tagging efficiency.

Finally, the high statistics of the measurement allow for an extraction of F_2^n after breaking up the data into different bins of spectator momentum. Based on the calculations shown in Fig. 8, the highest momentum spectators included in our analysis (90-100 MeV/c) have the largest off-shell corrections, predicted to be at the $\sim$2% level or below. By comparing the extracted structure function for the highest momentum spectators to those at lower momentum, we can set upper limits on the off-shell corrections. We can also look at somewhat higher momentum spectator protons to try and observe the larger corrections predicted above 100 MeV/c. This will be useful in testing the models, but projecting back down to the smaller spectator momenta will still require a model-dependent extrapolation, as opposed to our direct measurement of the spectator momentum dependence within our 60-100 MeV/c window.

5.3.5 Systematics uncertainties

In estimating our systematic uncertainties, we have several advantages compared to the BoNuS measurement. The SBS is a simpler spectrometer than CLAS, which has relatively large uncertainties associated with acceptance and trigger efficiency. In addition, BoNuS had a large contribution to the systematic associated with the model dependence associated with their extraction of F_2^d/F_2^p which was largely in the resonance region. The momentum resolution for the mTPC is an improvement over the resolution achieved in BoNuS and comparable to what was proposed for BoNuS12. Finally, as described above, we will have independent checks of the tagging efficiency rather than having to rely on a normalization against the extracted F_2^n/F_2^p at low x.

Based on the estimate of the previous TDIS proposals [25, 38], we assume a cross section uncertainty of $\sim$5% (see Sec. 3.2 of Ref. [25]). This is dominated by the SBS electron measurement has an uncertainty of $\sim$3%, including acceptance, efficiency, and PID uncertainty. In addition, we assume a $\sim$3% mTPC tagging/deadtime efficiency and 1-2% luminosity uncertainty.

6 Run Group Request

This run group proposal does not request any additional beamtime or changes in the experimental configuration to the E12-14-110 setup. We will use data from the proton and deuteron running to extract F_2^p and F_2^n and the tagged elastic n(e,e'n) data from the calibration run with neutrons detected in the HCAL.

7 Relationship to Other Experiments

Because of the broad physics enabled by inclusive measurements of e-n scattering there are several experiments which have overlap with either the physics case or experimental technique of the TDIS-n measurement. We discuss below the connection to these experiments.

- Experiment E12-10-002 [28] ran in Hall C and made inclusive measurements of F_2^p, F_2^d covering the large x and Q^2 region. One goal is to try and extract F_2^n, with a focus on larger Q^2 values. We cover a limited part of their kinematic region, but can extract F_2^n without relying on model to correct for nuclear effects in the deuteron, as the E12-10-002 data extend the Q^2 reach of high-x precision data, but will not improve on the uncertainties intrinsic to extraction of neutron for proton and deuteron.

- The TDIS-n extraction of F_2^n/F_2^p in the DIS region overlaps with MARATHON [52]. We do not extract the ratio in the DIS region above $x > 0.7$, which was the focus on MARATHON. Our measurement is complementary in that we use a different method to extract F_2^n for the free neutron, and provides a

measurement with very different systematic uncertainties, and provides an independent cross check of the normalization procedure used by MARATHON, as discussed in Sec. 5.3.4.

- The TDIS-n measurement has significant overlap with the BoNuS12 [2] experiment, which also aims to extract F_2^n over a wide range of x and Q^2 using proton spectator tagging. The largest difference is that the BoNuS12 measurement is focused on larger scattering angles to provide the high-Q^2 data to allow for extraction of F_2^n/F_2^p in the DIS region at the largest x values possible. While we do not provide a high-x measurement of F_2^n/F_2^p, this experiment will provide the ratio up to $x = 0.7$ and allow for a comparison using different tagging system. However, we can provide two independent checks of the tagging efficiency, which are not part of the BoNuS12 proposal, and in our kinematic phase space, the 5 days of running on deuterium will provide a factor of ∼7 increase in statistics compared BoNuS12. Our focus will be on the higher statistics measurements in the resonance region and for DIS up to $x = 0.7$, as well as the independent check of the tagging calibration and normalization procedures used in the BoNuS measurements.

- The ALERT [4] measurements on deuterium focus on measurements with large spectator momentum, but the ALERT tagging system should also have acceptance for low-momentum spectator tagging, and therefore has the potential to make similar measurements to BoNuS12 and TDIS-n. Compared to the BoNuS12 proposal, ALERT runs at a larger current (500 vs 200 nA) on a deuteron target with lower total thickness (30 cm at 3 atmospheres vs. 40 cm at 7.5 atmospheres), yielding an effective luminosity slightly below the BoNuS12 measurement. ALERT has 20 days of deuterium production running compared to 35 for BoNuS, and has the same minimum spectator momentum (70 MeV/c), so the final statistics should be roughly a factor of 2 below the proposed BoNuS12 measurement. As with BoNuS12, the ALERT measurement will have greater kinematic coverage than TDIS-n, in particular at large Q^2, but with a factor of ∼15 lower statistics compared to TDIS-n for the overlapping kinematics.

- Experiments E12-07-104 (CLAS) [53] and E12-09-109 (Hall A-SBS) [32] are approved to extract $G_{Mn}(Q^2)$ at high Q^2 from measurements of the ratio $d(e,e'n)/d(e,e'p)$. As with the 6 GeV CLAS measurement [3], these rely on a precise calibration of the neutron detection efficiency as a function of neutron momentum and a good understanding of the relative acceptance for detected protons and neutrons. In both cases, the approved measurements extend significantly higher in Q^2 than the TDIS-n measurement. These new measurements do have overlap with the existing CLAS data, as they both extend down to $Q^2 \approx 3$ GeV^2. However, the TDIS-n measurement will have greater overlap with both a large part of the CLAS data at 6 GeV and the approved 12 GeV experiments, while providing extractions of G_{Mn} with a completely different set of systematic uncertainties than both the 6 GeV and approved 12 GeV experiments.

- Experiments E12-11-107 [54] and E12-11-003A [55] are also approved to make measurements of DIS from a tagged nucleon in a deuteron target. However, while the experimental technique is very similar, these measurements focus on tagging of high-momentum spectators to examine off-shell effects in the region where they are large. They do not use detectors capable of low-momentum tagging, and so the physics of these measurements does not overlap the TDIS-n proposal.

8 Conclusions

We propose to measure electron-neutron inclusive scattering over a large kinematic region using the TDIS mTPC to tag low-momentum spectator protons. This acts as an effective free neutron target, allowing for a correction for the Fermi smearing of the neutron in the deuteron and, by choosing appropriate kinematics for the spectator proton, minimizing off-shell corrections and final-state interactions. In addition to providing

significantly improved statistics for the full kinematic range of our measurement, we provide measurements with very different systematic uncertainties compared to other neutron structure measurements. We will also be able to provide cross-checks of the tagging efficiency, not possible with previous JLab spectator tagging measurements, and use the high statistics of the data to verify that the off-shell corrections are as small as believed based on present calculations. The bullet list in the executive summary may be referred to for more details on the wealth of neutron structure topics we expect to be available in this electron-neutron inclusive scattering measurement, which we plan to study further with our data, in addition to the F_2^n extraction.

The neutron structure measurements can be performed using the same experimental setup and beamtime as in the TDIS proposal. We are examining the possibility of using the hadron calorimeter throughout the run period as an additional calibration, and know of no reason why this would adversely impact the approved TDIS measurements. However, this is not required for the extraction as described in this proposal, and so the physics presented here will not be limited if this does not turn out to be feasible.

References

[1] D. Abrams et al. Measurement of the Nucleon F_2^n/F_2^p Structure Function Ratio by the Jefferson Lab MARATHON Tritium/Helium-3 Deep Inelastic Scattering Experiment. *arXiv:2104.05850*, 2021.

[2] The structure of the free neutron at large x-Bjorken. `https://www.jlab.org/exp_prog/proposals/06/PR12-06-113.pdf`. JLab PAC30 (2006).

[3] J. Lachniet et al. A Precise Measurement of the Neutron Magnetic Form Factor G_{Mn} in the Few-GeV^2 Region. *Phys. Rev. Lett.*, 102:192001, 2009.

[4] Tagged EMC Measurements on Light Nuclei. `https://www.jlab.org/exp_prog/proposals/17/PR12-17-012A.pdf`. JLab PAC45 (2017).

[5] R. Abdul Khalek et al. Science Requirements and Detector Concepts for the Electron-Ion Collider: EIC Yellow Report. *arXiv:2103.05419*, 2021.

[6] J. Arrington et al. Revealing the structure of light pseudoscalar mesons at the Electron-Ion Collider. *arXiv:2102.11788*, 2021.

[7] J. D. Bjorken. Asymptotic Sum Rules at Infinite Momentum. *Phys. Rev.*, 179:1547–1553, 1969.

[8] J. D. Bjorken and Emmanuel A. Paschos. Inelastic Electron Proton and gamma Proton Scattering, and the Structure of the Nucleon. *Phys. Rev.*, 185:1975–1982, 1969.

[9] Richard P. Feynman. Very High-Energy Collisions of Hadrons. *Phys. Rev. Lett.*, 23:1415–1417, Dec 1969.

[10] A. Accardi, L. T. Brady, W. Melnitchouk, J. F. Owens, and N. Sato. Constraints on large-x parton distributions from new weak boson production and deep-inelastic scattering data. *Phys. Rev. D*, 93:114017, 2016.

[11] Shujie Li. Extracting Neutron Structure Functions from CJ15. `https://indico.cern.ch/event/761382/contributions/3179462/attachments/1750564/2836367/Extracting_Neutron_Structure_Functions_from_CJ15.pdf`. CTEQ Workshop JLAB: Parton Distributions as a Bridge from Low to High Energies (2018).

[12] J. Arrington, J. G. Rubin, and W. Melnitchouk. How Well Do We Know The Neutron Structure Function? *Phys. Rev. Lett.*, 108:252001, 2012.

[13] A. Accardi, W. Melnitchouk, J. F. Owens, M. E. Christy, C. E. Keppel, L. Zhu, and J. G. Morfin. Uncertainties in determining parton distributions at large x. *Phys. Rev. D*, 84:014008, 2011.

[14] N. Baillie et al. Measurement of the neutron F2 structure function via spectator tagging with CLAS. *Phys. Rev. Lett.*, 108:142001, 2012. [Erratum: Phys.Rev.Lett. 108, 199902 (2012)].

[15] A. Bodek et al. Experimental Studies of the Neutron and Proton Electromagnetic Structure Functions. *Phys. Rev. D*, 20:1471–1552, 1979.

[16] Glennys R. Farrar and Darrell R. Jackson. Pion and Nucleon Structure Functions Near x=1. *Phys. Rev. Lett.*, 35:1416, 1975.

[17] W. Melnitchouk and Anthony William Thomas. Neutron / proton structure function ratio at large x. *Phys. Lett. B*, 377:11–17, 1996.

[18] Craig D. Roberts, Roy J. Holt, and Sebastian M. Schmidt. Nucleon spin structure at very high-x. *Phys. Lett. B*, 727:249–254, 2013.

[19] L. L. Frankfurt and M. I. Strikman. Hard Nuclear Processes and Microscopic Nuclear Structure. *Phys. Rept.*, 160:235–427, 1988.

[20] W. Melnitchouk, M. Sargsian, and M. I. Strikman. Probing the origin of the EMC effect via tagged structure functions of the deuteron. *Z. Phys. A*, 359:99–109, 1997.

[21] Misak Sargsian and Mark Strikman. Model independent method for determination of the DIS structure of free neutron. *Phys. Lett. B*, 639:223–231, 2006.

[22] Silvano Simula. Semiinclusive deep inelastic electron scattering off the deuteron and the neutron to proton structure function ratio. *Phys. Lett. B*, 387:245–252, 1996.

[23] S. Tkachenko et al. Measurement of the structure function of the nearly free neutron using spectator tagging in inelastic ^{2}H(e, e'p)X scattering with CLAS. *Phys. Rev. C*, 89:045206, 2014. [Addendum: Phys.Rev.C 90, 059901 (2014)].

[24] K. A. Griffioen et al. Measurement of the EMC Effect in the Deuteron. *Phys. Rev. C*, 92:015211, 2015.

[25] Measurement of Tagged Deep Inelastic Scattering (TDIS). `https://www.jlab.org/exp_prog/proposals/15/PR12-15-006.pdf`. JLab PAC43 (2015).

[26] J. Arrington and N. Fomin. Searching for flavor dependence in nuclear quark behavior. *Phys. Rev. Lett.*, 123(4):042501, 2019.

[27] X. G. Wang, A. W. Thomas, and W. Melnitchouk. Do short-range correlations cause the nuclear EMC effect in the deuteron? *Phys. Rev. Lett.*, 125:262002, 2020.

[28] Precision measurements of the F_2 structure function at large x in the resonance region and beyond. `https://www.jlab.org/exp_prog/proposals/10/PR12-10-002.pdf`. JLab PAC35 (2009).

[29] A. V. Klimenko et al. Electron scattering from high-momentum neutrons in deuterium. *Phys. Rev. C*, 73:035212, 2006.

[30] S. Liuti and Franz Gross. Extraction of the ratio of the neutron to proton structure functions from deep inelastic scattering. *Phys. Lett. B*, 356:157–162, 1995.

[31] V. Palli, C. Ciofi degli Atti, L. P. Kaptari, C. B. Mezzetti, and M. Alvioli. Slow Proton Production in Semi-Inclusive Deep Inelastic Scattering off Deuteron and Complex Nuclei: Hadronization and Final State Interaction Effects. *Phys. Rev. C*, 80:054610, 2009.

[32] Precision Measurement of the Neutron Magnetic Form Factor up to $Q^2 = 18.0$ (GeV/c)^2 by the Ratio Method. `https://www.jlab.org/exp_prog/proposals/09/PR12-09-019.pdf`. JLab PAC34 (2009).

[33] Measurement of the Neutron Electromagnetic Form Factor Ratio G_E^n/G_M^n at High Q^2. `https://www.jlab.org/exp_prog/proposals/09/PR12-09-016.pdf`. JLab PAC34 (2009).

[34] Large Acceptance Proton Form Factor Ratio Measurements at 13 and 15 (GeV/c)^2 Using Recoil Polarization Method. `https://www.jlab.org/exp_prog/proposals/07/PR12-07-109.pdf`. JLab PAC33 (2007).

[35] Measurement of Semi-Inclusive Pion and Kaon electroproduction in the DIS Regime on a Transversely Polarized ^{3}He Target using the Super BigBite and BigBite Spectrometers in Hall A. `https://www.jlab.org/exp_prog/proposals/09/PR12-09-018.pdf`. JLab PAC34 (2009).

[36] B. A. Mecking et al. The CEBAF Large Acceptance Spectrometer (CLAS). *Nucl. Instrum. Meth. A*, 503:513–553, 2003.

[37] N Akopov et al. The HERMES dual-radiator ring imaging Cherenkov detector. *Nucl. Instrum. Meth. A*, 479:511–530, 2002.

[38] Measurement of Kaon Structure Function through Tagged Deep Inelastic Scattering (TDIS). `https://www.jlab.org/exp_prog/proposals/17/C12-15-006A.pdf`. JLab PAC45 (2017).

[39] ALICE Upgrade of the Readout & Trigger System - Technical Design Report. `http://cds.cern.ch/record/1603472/files/ALICE-TDR-015.pdf`.

[40] J. Adolfsson et al. SAMPA Chip: the New 32 Channels ASIC for the ALICE TPC and MCH Upgrades. *JINST*, 12:C04008, 2017.

[41] E. Jastrzembski, D. Abbott, J. Gu, V. Gyurjyan, G. Heyes, B. Moffit, E. Pooser, C. Timmer, and A. Hellman. SAMPA Based Streaming Readout Data Acquisition Prototype. In *22nd IEEE Real Time Conference*, 2020.

[42] J. W. Lightbody and J. S. O'Connell. Modeling single arm electron scattering and nucleon production from nuclei by GeV electrons. *Comput. Phys.*, 2(3):57, 1988.

[43] A. Puckett. unpublished. See `https://hallaweb.jlab.org/wiki/index.php/Documentation_of_g4sbs`, 2016.

[44] Pavel M. Nadolsky, Hung-Liang Lai, Qing-Hong Cao, Joey Huston, Jon Pumplin, Daniel Stump, Wu-Ki Tung, and C. P. Yuan. Implications of CTEQ global analysis for collider observables. *Phys. Rev. D*, 78:013004, 2008.

[45] P. E. Bosted and M. E. Christy. Empirical fit to inelastic electron-deuteron and electron-neutron resonance region transverse cross-sections. *Phys. Rev. C*, 77:065206, 2008.

[46] L. M. Stuart et al. Measurements of the delta (1232) transition form-factor and the ratio sigma-n / sigma-p from inelastic electron - proton and electron - deuteron scattering. *Phys. Rev. D*, 58:032003, 1998.

[47] W. Melnitchouk, R. Ent, and C. Keppel. Quark-hadron duality in electron scattering. *Phys. Rept.*, 406:127–301, 2005.

[48] J. Arrington, R. Ent, C. E. Keppel, J. Mammei, and I. Niculescu. Low Q scaling, duality, and the EMC effect. *Phys. Rev. C*, 73:035205, 2006.

[49] I. Niculescu, J. Arrington, R. Ent, and C. E. Keppel. Moments of nuclear and nucleon structure functions at low Q^2 and the momentum sum rule. *Phys. Rev. C*, 73:045206, 2006.

[50] S. P. Malace, Y. Kahn, W. Melnitchouk, and C. E. Keppel. Confirmation of quark-hadron duality in the neutron Faa(2) structure function. *Phys. Rev. Lett.*, 104:102001, 2010.

[51] I. Niculescu et al. Direct observation of quark-hadron duality in the free neutron F_2 structure function. *Phys. Rev. C*, 91(5):055206, 2015.

[52] MeAsurement of the F_2^n/F_2^p, d/u RAtios and $A = 3$ EMC Effect in Deep Inelastic Electron Scattering Off the Tritium and Helium MirrOr Nuclei. http://hallaweb.jlab.org/collab/PAC/PAC37/C12-10-103-Tritium.pdf. JLab PAC36 (2010).

[53] Measurement of the Neutron Magnetic Form Factor at High Q2 Using the Ratio Method on Deuterium. https://www.jlab.org/exp_prog/proposals/07/PR12-07-104.pdf. JLab PAC32 (2007).

[54] In Medium Nucleon Structure Functions, SRC, and the EMC effect. https://www.jlab.org/exp_prog/proposals/11/PR12-11-107.pdf. JLab PAC38 (2011).

[55] In Medium Proton Structure Functions, SRC, and the EMC effect. https://www.jlab.org/exp_prog/proposals/11/PR12-11-003A.pdf. JLab PAC43 (2015).